17th World Conference on Earthquake Engineering, 17WCEE
Sendai, Japan - September 13th to 18th 2020

HETEROGENEOUS MULTICYCLE DYNAMIC RUPTURE MODELING FOR A VERTICAL STRIKE-SLIP FAULT

P. Galvez[1,2], A. Petukhin[3], P. Somerville[4], K. Miyakoshi[5], K. Irikura[6], and D. Peter[7]

(1) *Visiting researcher, ETH Zurich, Earth Science, Switzerland,* percy.galvez.barron@gmail.com
(2) *Researcher, KAUST University, Saudi Arabia,* percy.galvez.barron@gmail.com.
(3) *Senior researcher, Geo-Research Institute, earthquake engineering, Osaka, Japan,* anatolyp@geor.or.jp
(4) *Principal Seismologist, AECOM, Los Angeles, United States,* paul.somerville@aecom.com
(5) *Group leader, Geo-Research Institute, earthquake research, Osaka, Japan,* ken@geor.or.jp
(6) *Adjunct Professor, Aichi Institute of Technology, Japan,* irikura@geor.or.jp
(7) *Assistant Professor, KAUST University, Saudi Arabia,* daniel.peter@kaust.edu.sa

Abstract

Dynamic rupture modelling is necessary for estimating parameters that are poorly resolved by seismic source inversion, such as rupture velocity and slip rate function. Source inversions using forward dynamic modelling are used to obtain rupture models, but their stress and strength heterogeneities are prescribed arbitrarily. In this study, to generate large number of physically self-consistent rupture models whose rupture process is consistent with the spatio-temporal heterogeneity of past earthquakes, we use multicycle simulations under the rate-and-state friction law. Using the case of the 1992 Landers earthquake, we demonstrate that this random approach can generate rupture models reproducing the observed slip, rupture velocity and ground motions, thereby accomplishing in effect a dynamic source inversion [1].

To get a realistic irregular seismic sequence, several realizations of 2D correlated heterogeneous random distributions of characteristic weakening distance "*Dc*" in rate and state friction are tested. The quasi-dynamic solver QDYN was used to nucleate the seismic events and SPECFEM3D to resolve the rupture process. Other important parameters are the normal stress, which controls the stress drop and rupture velocity during an earthquake, and the maximum value of the *Dc* distribution, that controls rupture velocity but not stress drop. Following these ideas, we performed a parametrization study (iteratively with [2]) by full-dynamic rupture modeling. Then, set of a hundred spontaneous source models was generated in a wide magnitude range (*Mw*5.5-7.5).

In a companion paper [2], we validated source models by comparing the source scaling relations vs. seismic moment with results from the source inversions. We also found that ground motions from our models agree well with the ground motion prediction equation (GMPE) values.

Keywords: earthquake dynamics, source characterization, strong ground motion prediction

1. Introduction

Due to the lack of dense recordings of strong ground motions in the vicinity of faults, physics-based numerical modeling is a necessary tool for the assessment of variability of strong ground motions in potentially devastating large earthquakes. In a simulation-based seismic hazard analysis, it is critical to be able to generate a large number of physically self-consistent source models whose rupture process captures the main physics of earthquake rupture. Such a set of source models can be used for verification of assumptions underlying strong ground motion simulation schemes (e.g. [3]) and for constraining seismic source inversion. The approach involves developing models based on idealized friction laws, slip-weakening or rate-and-state (RS) friction, to examine the impact of assumed statistical characteristics of heterogeneities.

Usually, such efforts are based on single-rupture dynamic models in which heterogeneous distributions of fault stress and strength are prescribed quite independently. However, stress and strength heterogeneities cannot be prescribed arbitrarily. Their inter-dependence must be consistent with a mechanical model of deformation and stress evolution over the longer time scale of the earthquake cycle. For instance, it is expected that stress concentrations can develop at the edges of asperities, introducing a correlation between stress and strength that enhances high frequency radiation at asperity edges.

Therefore, to enable the generation of initial stresses for dynamic rupture models that are consistent with the distribution of fault strength and fault geometry, we employ earthquake cycle modeling (e.g. [4] and references therein, [5]). Our approach involves producing earthquakes based on the RS friction law in order to examine the impact of assumed statistical characteristics of heterogeneities (e.g. [6, 7]). The earthquake cycle is modelled using a quasi-dynamic solver under the RS friction [8, 9, 10]. Each simulation assumes a 2D distribution of the characteristic weakening distance Dc in RS friction, and depth dependent frictional parameters a and b. The dynamic rupture parameters (initial stresses, Dc, a, b and the state) extracted from the multi-cycle simulations are then used as input parameters in fully-dynamic single-event rupture modelling using SPECFEM3D [11, 12] with the same RS friction law. Considering seismic wave generation and propagation, fully-dynamic simulations improve the consistency of transient stress changes in front of the rupture tip, and improves the accuracy of simulated models in comparison with quasi-dynamic cycle simulations in previous works (see [4, 7, 13] and references therein).

In contrast to previous works, multi-cycle simulations in this study employ RS friction laws both in quasi-dynamic and full-dynamic modelling. We do not prescribe the simplified slip-weakening (SW) friction law [14, 15] that was used in earlier full-dynamic simulations, e.g. [16, 17]. However, slip-weakening phenomena appears spontaneously in these simulations [18]. This helps us to obtain a well validated event dataset see [2] that can be used to investigate the dynamic rupture characteristics of each single event (which may be poorly resolved by source inversion, e.g. slip rate functions, rupture velocities, etc. [19, 20]).

In previous studies [1] we performed simulations on the multi-segment Landers fault system. The strike variations of the faults involved lead to natural segmentation, which is necessary for the simulation of a broad magnitude range of earthquakes. The fault segmentation brings complexity into the rupture process. For instance, the change of strike between fault segments enhances strong variations of stress. We succeeded in generating a set of earthquake models that cover a broad range of magnitudes: Mw=7.0~7.8. In order to validate simulation results, we demonstrate that this random approach can generate rupture models that reproduce the observed slip, rupture velocity and ground motions, thereby accomplishing, in effect, a dynamic source inversion.

The main goal of this study is to find those parameters of multi-cycle simulations (frictional parameters as well as fault parameters) that will allow us to get well validated rupture models that reproduce well documented features of observed earthquakes: source scaling, ground motions and permanent surface slip. In order to find proper parameter settings, we made a case study. To get a broad range of self-arrested ruptures we test different distributions of Dc, following the studies [7, 21]. Unfortunately, due to the large cost of simulations, our case study lacked a systematic search, and the selection of cases was driven by previous studies, by our experience, and by analysis of previous cases.

Prediction of strong ground motions starts from estimation of the source area *S* from fault length *L* and seismogenic width *Wseis*. Then, a scaling relation between *S* and *Mo* is used for estimation of *Mo* for a possible future earthquake, which defines other necessary parameters, e.g. [22]. For this reason, we choose reproducing the observed scaling as a primary target for selection of the friction model. The target for this study is the transition between the 1st and 2nd stages (magnitude range *Mw* = 6-7) of the 3-stage scaling proposed in [3]. Additionally, we tune the near surface friction model by comparing permanent surface slip with field observations. In a companion study [2], in order to further validate our best model, the ground motions are simulated using dynamic ruptures, and their parameters are compared against Ground Motion Prediction Equation models (GMPE's). Finally, we investigate kinematic rupture characteristics, such as the spatial correlations of large slip and high slip-rate areas, source time functions, and rupture velocities, which are poorly resolved by the source inversion,.

2. Earthquake multi-cycles

For earthquake cycle modelling we adopt the RS friction law and solve the quasi-dynamic cycle problem with a boundary element method with adaptive time stepping (QDYN, [13]). Once an earthquake is nucleated and reaches seismic slip velocities (> 0.1 m/s), QDYN exports the stresses and friction parameters to a rupture dynamic solver based on the spectral element method with fixed time step (SPECFEM3D, [11, 12]) to properly resolve the rupture process. However, we adopt a one-way coupling approach: we do not import the outputs of SPECFEM3D back to QDYN.

An important feature is that in our simulations with adaptive time stepping we naturally nucleate the rupture, and the time step is decreased gradually to resolve the nucleation processes. Another advantage is that the initial stresses for the dynamic rupture modelling capture the stress evolution generated by previous events. In contrast to previous single-rupture full-dynamic modelling (e.g. [23]) we do not apply any artificial procedure to accelerate the rupture initiation. Such procedures require the rupture initiation zone of a large size and greatly increase the lower magnitude limit of simulated earthquakes. However, many small magnitude earthquakes are necessary to generate heterogeneous stress and strength fields on the fault. QDYN is switched to SPECFEM once the slip rate reaches 0.1 m/s in the rupture initiation zone. The nucleation process starts before the slip rate reaches this threshold, but we do not expect that this affects aspects of the eventual rupture that are important for strong motion simulation.

2.1 Fault Geometry and Mesh

The fault model used in our study is a vertical strike-slip planar fault. This type of fault is prevalent in western Japan, as well as in the western USA and many other regions. In order to reduce the computation cost for simulation of small earthquakes, which require smaller mesh size, we limit the fault size to 128km.

In order to mesh the complex fault systems in previous studies [1, 24], as well as edges of the planar fault in this study, we made use of CUBIT, a state-of-the-art hexahedral mesh generation software. The mesh and the fault used in this study are shown in Fig.1. During the rupture process, 3 to 5 grid points are needed to resolve the cohesive zone. As the cohesive zone is proportional to *Dc*, the minimal *Dc* values available for modeling depend on the minimum grid size. In order to allow smaller *Dc* values, thus smaller nucleation area and event magnitude, we refine the mesh size along the fault. This refinement allows accurate modeling of the rupture without greatly increasing the need for computer resources, while inducing only minor disturbance on the wave propagation modeling. The grid size of the refined fault elements is about 125 m.

2.2 Friction Parameters

Fig.1 also shows initial parameters of the RS friction: the *a-b* and normal stress σ values as a function of depth. The region of (*a-b*) < 0 defines the area of velocity weakening, where both small and large events nucleate. The reference friction coefficient (μ_o) is 0.6 and the loading rate (V_{pl}) 5mm/yr. The seismogenic zone goes down to 15 km depth. Large ruptures may propagate into nearby regions with (*a-b*) > 0. The normal stress increases linearly from 0 to 6 km depth, then saturates at 75 MPa due to the existence of

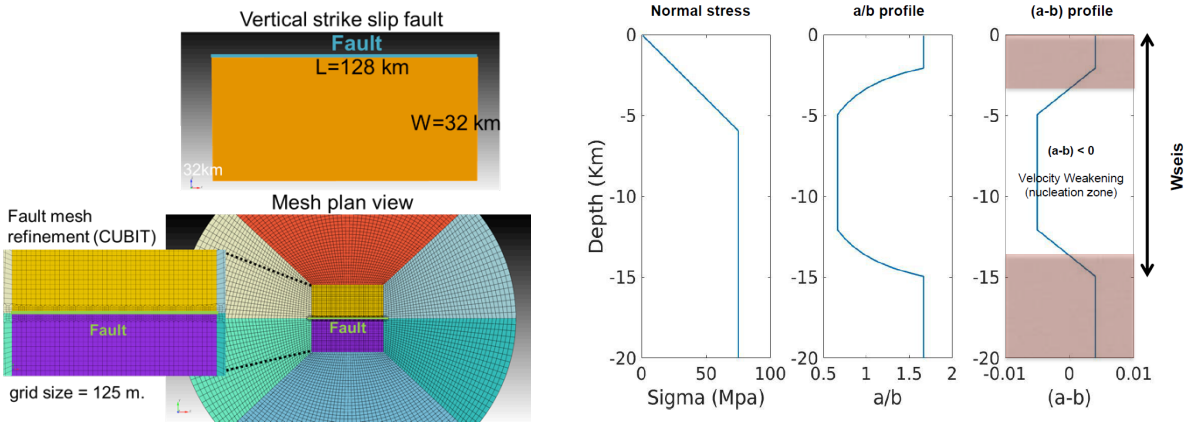

Fig. 1 – Left: Fault dimensions and fault mesh. Right: Friction settings for Cases 1 and 2.

overpressure fluids, e.g. [25, 26]. Our initial setting of the saturated normal stress is similar to [13], 75 MPa, but larger than in [7], 50 MPa. For the *Dc* settings we made additional detailed study below.

2.2.1 On the Irregular Seismicity Range of *Dc*

From the fault friction point of view, there are two types of earthquake faults: mature and immature. Mature faults experience many earthquakes repeatedly rupturing the same segment of the fault, smoothing out friction heterogeneities and reducing the *Dc* range. Characteristic earthquakes are expected for mature faults. The characteristic events are considered to be those that rupture repeatedly on approximately the same fault area, and have about the same magnitude, but not necessary the same final slip distribution or rupture nucleation point. [1] used a characteristic seismicity pattern in order to get an event that could reproduce major features of the target 1992 Landers earthquake, using friction settings for mature faults. However, for this study, in order to get earthquakes in a wide magnitude range we need a realistic irregular seismic pattern and immature fault settings having a larger range of *Dc* values.

In order to get irregular seismicity, first of all we employ a realistic von Karman distribution of *Dc* spatial heterogeneities. From an analysis of final slip from a series of source inversion models with different magnitudes (*Mw* = 5.9 - 8.0), in [27] it is found that the slip distribution followed a von Karman auto-correlation (VKA) function which is associated with a characteristic correlation length. Following these results and similar to [7] we applied the VKA to generate irregular seismicity. Another important parameter is the probability distribution (histogram) of *Dc* values. Two kinds of probability distribution of *Dc* are frequently used in multicycle simulations: uniform and log-normal. As explained in [7] we expect irregular seismicity for the uniform model, while simulations in [1] with log-normal distribution resulted in characteristic seismicity.

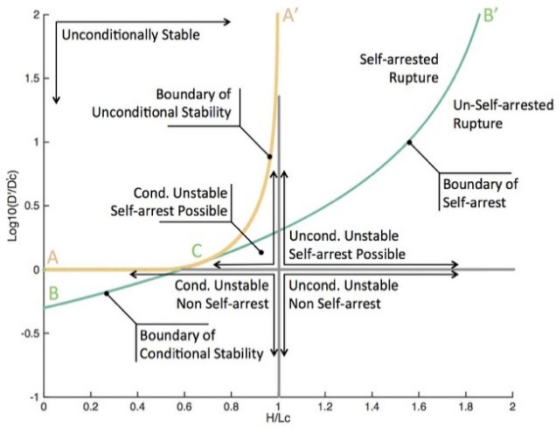

Fig.2 – Theoretically different seismicity regimes

Detailed study of the effects of distribution of *Dc* values on the seismicity pattern is made in [21]. To analyze different seismicity types for our models, they proposed a reduced model (RC) with only one asperity, which consists of a region of minimum *Dc* and linear gradients *D'* at the edges of the asperity. By performing 1D simulations of the RC model, they found regions of irregular seismicity occurring at the transition regime from aseismic to seismic slip. By analysis of the unstable condition ($H > Lc$, where H is asperity size and Lc is a critical nucleation length) for the reduced model, in [21] it is found theoretically different seismicity regimes, see Fig.2.

2.2.2 *Dc* distribution for irregular seismicity

Guided by the irregular seismicity region for the RC model in the previous section, here we prescribe values of *Dc* truncated by a minimum $Dc = 0.005$ and maximum $Dc = 0.1$ and explore different *Dc* regimes. In practice the fault rheology is more irregular than the RC model and contains many asperities of different sizes. For 2D faults, we found regions of irregular seismicity nucleating everywhere along the fault due to large values of standard deviation of *Dc* (0.005 to 1.0) and short correlation length ($Lcor < 4$ Km). In [7] also reported regimes of irregular seismicity at large values of standard deviation, which corresponds to uniform distribution, and values of correlation length $Lcor < 4$ Km.

Based on these studies we test the *Dc* distributions listed in Table 1. In a practical sense, our models can be interpreted as the combinations of many reduced models. As a result, we expect more irregular seismicity in our models than the reduced model in [21] predicts. The effective *Dc* gradient scales with the standard deviation *std* and the correlation length *Lcor* with the minimum region of *Dc*. Fig.3 shows the *Dc* distribution from the models for Cases 1 and 2 in Table 1. In our models the mean of log10(*Dc*) is equal to -1.65 and has uniformly distributed *Dc*.

Table 1 – Main parameters of the studied cases

Case number	**Range of *Dc* (m)**	**Distribution of *Dc***	**Correlation length *Lcor* (km)**	**Normal stress σ (MPa)**	**Near surface cohesion***
Case 1	0.005-0.1	Uniform (allow irregular seismicity)	1.0	75	4MPa
Case 2	0.005-0.1		2.0	75	4MPa
Case 3	0.005-0.075		1.0	50	4MPa
Case 4	0.005-0.075		2.0	50	4MPa
Case 5	0.005-0.075		2.0	50	none

* Near surface 2km cohesion zone is promotes rupture arrest but generates some free oscillations. Stronger cohesion prevents rupture penetration to the ground surface.

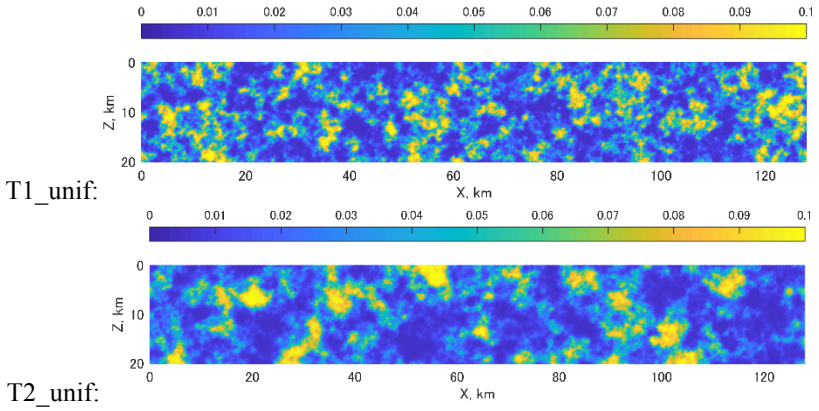

Fig.3 – *Dc* distribution for Cases in Table 1. T1_unif and T2_unif correspond to von Karman models with correlation length *Lcor* = 1km and 2km respectively, and uniformly distributed.

3. Parametrization study of earthquake cycles

In this study we tested 5 cases (see Table 1). Selection of friction parameters was driven by previous studies and by our experience, compiled in Table 2. We started from two cases of *Dc* distributions and analyzed them. Then, in order to get better fitting between simulated and observed scaling, we changed the normal stress. The next parameters tested were the seismogenic width and shallow cohesion settings.

We use the agreement between observed and simulated scaling relations *S*(*Mo*) as a primary criterion for parameter setting in our multicycle modelling. For observed scaling *S*(*Mo*) we use the 3-stage scaling relationship [3]. This scaling relation is based on the results of the seismic inversion of ground motions, and is perfectly fit to the problem of forward prediction of strong ground motions. The 1st stage was proposed in [28] and reflects self-similarity of relatively small ruptures. In the 2nd stage at $Mw > 6.5$ ruptures reach the boundaries of the seismogenic layer and transition from self-similar to elongated width-saturated ruptures (W-model, [22]). The 3rd stage was added in [3] for large ruptures $Mw > 7.5$ having saturated *Dave* values (D-model). The quasi-dynamic cycle modelling of [13] clearly reproduces the transition to the 3rd stage. They also proposed a theoretical interpretation for transition from 1st to 2nd stage, but modelling results question its reliability (T.Iwata, personal communication). In this study we focus on this transition.

Another important criterion is agreement between ground motions simulated by the multicycle ruptures and observed ground motions (GM). We noticed that agreement between simulated and observed *Vr* enhances the agreement between simulated and observed GMs. This approach helped us to get rupture models that reproduce the GMs of the 1992 Landers earthquake in just a few iterations, see [1]. For this reason, our second criterion for parameter settings is to keep rupture velocity at a level of $Vr \sim 2.8$ km/s.

Parameter settings for Cases 1 and 2 are driven by the discussion in Paragraph 2.2.2. Case 3 allows the average stress drop of the rupture to be reduced and improves the agreement with observed scaling *S*(*Mo*), while keeping rupture velocity at a level of 2.8 km/s. These cases are for *Wseis* = 15km, similar to [1]. In Case 4 we change *Wseis* to 18km, similar to the average fault width of strike-slip earthquakes in Japan. However, we found that due to shallow cohesion that is too strong, ruptures do not reach the surface, and the permanent slip at the surface disagrees with observed values. For this reason, we also run Case 5 without shallow cohesion. Our best target case is Case 5.

Table 2 – Possible effects of the friction parameter settings

Name of the tested parameter	**Possible Effect**	**Effect of parameter <u>increase</u>**	**Effect of parameter <u>decrease</u>**
Std of *Dc* distribution	Controls seismic irregularity	Irregular	Characteristic
Correlation length, *Lcor*	Controls seismic irregularity and stress heterogeneity	Decreases number of small events Decreases clustering	Increases number of small events Increases clustering
Dc cut-off, *Dc_max*	Controls rupture velocity *Vr* and magnitude *Mw*	Decreases *Vr* and *Mw*	Increases *Vr* and *Mw*
Normal stress, σ	Controls stress drop Δσ and *Vr*	Δσ increases *Vr* increases	Δσ decreases *Vr* decreases
Strength of near surface *a-b* and cohesion settings	Controls rupture penetration to the surface	Leads to buried ruptures, *Mw* decreases	Leads to surface ruptures, *Mw* increases

4. Simulation results

We generated about 100-150 events for each of Cases 1-5. The simulated events span a magnitude range of *Mw* 5.5-7.5 (e.g. see Fig.4) that correspond to the 1st and 2nd stages in the source scaling relationship assumed by [3]. Examples of distribution of the peak slip, peak slip rate, rupture time and stress drop are shown in Fig.5. Unfortunately, some ruptures have unnatural artefacts: e.g. double ruptures or edge-arrested ruptures, see examples in Fig.6. We deleted them and analyzed the remaining 50-75 ruptures for each case. For details of the screening process see [2].

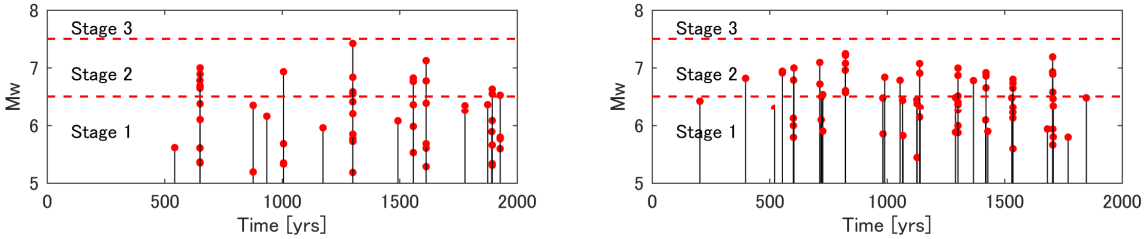

Fig.4 – Distribution of simulated events with time for Case 1 (left) and Case 2 (right). First 500 years is the loading and warm-up stage where no events were generated.

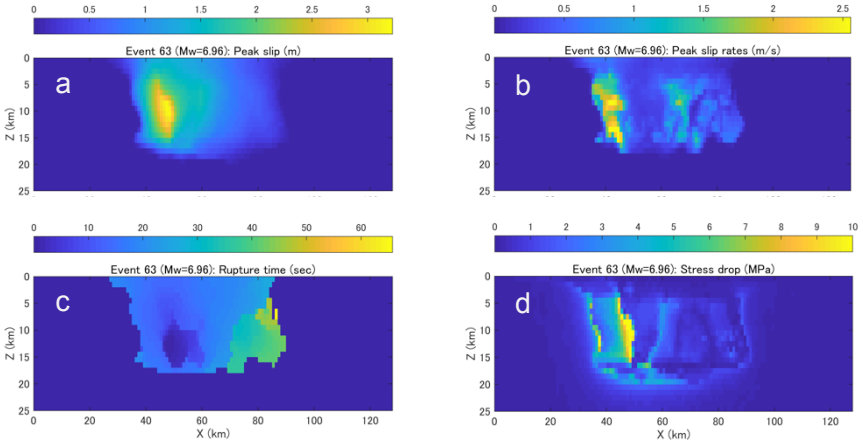

Fig.5 – Example of peak slip (a), peak slip rate (b), rupture time (c) and stress drop (d) distributions for *Mw*6.96 event.

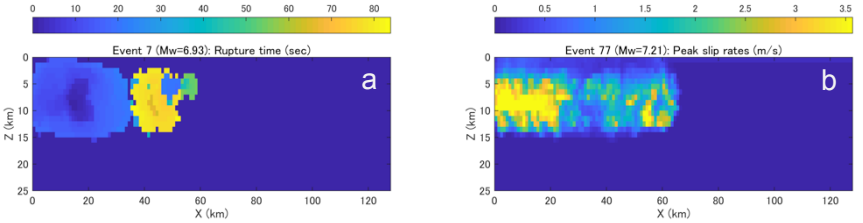

Fig.6 – Examples of (a) rupture time distribution for the double rupture event and (b) peak slip-rate distribution for the edge-arrested event

4.1 Ruptures for Case 1 and 2

The objective of the simulations in Cases 1 and 2 is to find parameters for irregular seismic regime (in the case of full-dynamic ruptures). In order to analyze the irregularity of the seismic regime, we plot ruptures vs. time and *Mw*; see Fig.4. Ruptures for both cases have a large magnitude range, which indicates the irregularity of the seismic regime. However, the Case 1 ruptures are strongly clustered in time. The Case 2 ruptures with larger *Lcor* are less clustered: for example, for Case 2 there are four clusters in the interval

1200-1400 yrs., but only one for Case 1 in the same time interval. However, Case 2 has a smaller magnitude range.

Scaling of rupture area *S* and average slip *Dave* vs. seismic moment *Mo* is shown in Fig.7. Criteria and trimming procedures, proposed in [28], are used to estimate *S* and *Dave*. The gradient of *S*-values clearly shows the existence of a transition between Stage 1 and Stage 2, while absolute values of *S* are underestimated a little. Scaling of *Dave* vs. *Mo* also shows the existence of a transition between Stage 1 and Stage 2. However, the absolute values of *Dave* are overestimated a little.

Finally, we investigated average stress drop Δσ values on the ruptures. On average, Δσ does not change with increasing magnitude through the transition, although the scatter of their values is large. The estimated average is 4.2 MPa for Case 1 and 4.7 MPa for Case 2. In [29] it is found that observed scaling *S*(*Mo*) can be explained by stress drop Δσ = 3.1 MPa for intraplate earthquakes. Δσ values here are much larger than estimated in [29]. Large Δσ values are consistent with underestimated scaling for *S* and overestimated scaling for *Dave*. From the results for Cases 1-2 we expect that decreasing Δσ could also improve the scaling with *S*.

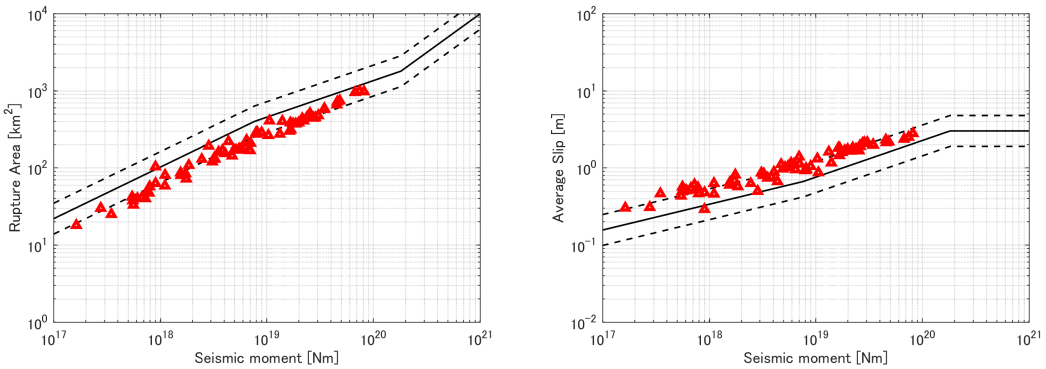

Fig.7 – Scaling of the rupture area *S* (left) and average slip *Dave* (right) for Cases 1 and 2

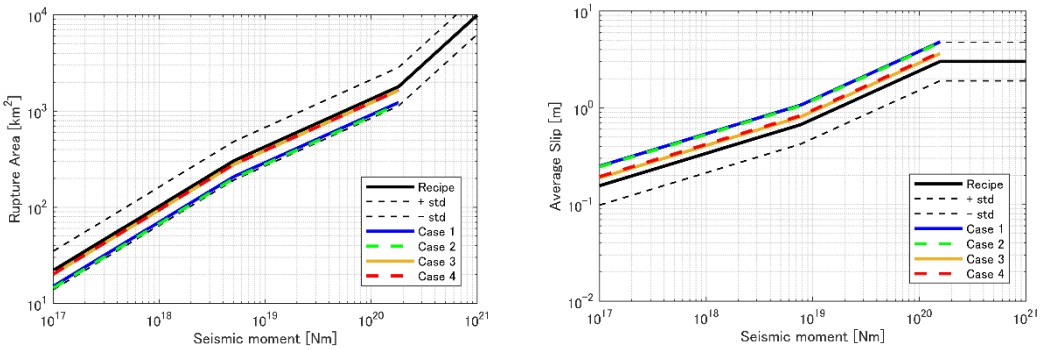

Fig.8 – Comparison of average residuals of the rupture area *S* (left) and average slip *Dave* (right) for Cases 1-4 with the observed scaling (black line). Due to reduced normal stress σ, Cases 3 and 4 have reduced Δσ and better fit to the observed scaling [3].

4.2 Ruptures for Case 3 and 4

The objective of simulations in Case 3 is to tune parameters to get smaller stress drop values and improve source scaling accordingly. According to [30], stress drop $\Delta\sigma$ can be tuned by tuning normal stress, and/or friction parameters *a* and *b*:

$$\Delta\sigma = \sigma\left[(b-a)\ln\left(\frac{V}{V_{bg}}\right) - b\ln w\right] \quad (1)$$

where σ - normal stress, V_{bg} - background velocity. $w = VQ/Dc$. Once the rupture passes through, w equals 1, therefore ln(w) can be neglected.

We tried to tune both the *b-a* value and the normal stress. Tuning of σ was easier and more effective and the major change in Case 3 is the reduced normal stress from 75MPa to 50MPa. However, reducing normal stress also results in reducing the rupture velocity *Vr* and may result in underestimation of GM amplitudes. In order to keep rupture velocity at the observed level *Vr* = 2.8 km/s, we also reduced *Dc_max* by 25% in Case 3.

The average scaling of *S* vs. *Mo* for these cases, and comparison with Cases 1 and 2, are shown in Fig.8. Absolute values of *S* become larger and better agree with observed scaling, while the gradients stay in agreement with Stage 1 and Stage 2. The average scaling of *Dave* vs. *Mo* and comparison with Cases 1 and 2 are also shown in Fig.8. As expected, average Δσ become smaller: the estimated average is 3.2 MPa for Case 3. This value is almost the same as found in [29] and assumed by [3]. As an indicator of decreased Δσ values, absolute values of *Dave* become smaller and better agree with observed scaling, while the gradients stay in agreement with Stage 1 and Stage 2.

As for Case 4, due to the change of seismogenic width to a value typical in Japan, *Wseis* = 18km, *W*-values are saturated at *W* = 18km in large magnitudes [2].

4.3 Ruptures for Case 5

Although ruptures in Case 3 have good fit with observed scaling and Case 4 has *Wseis* adjusted to the target region, comparison of permanent surface offset with observed values (e.g. [31]) shows that they are largely underestimated. This is due to a strong barrier near the surface that does not allow ruptures to penetrate to the surface. For this reason, in Case 5 we tried to remove this burrier by reducing near surface cohesion to zero. This did not change the scaling relations *S*(*Mo*) and *Dave*(*Mo*) on average but increased the permanent rupture offset.

In Fig.9 we compare maximum permanent rupture offset *Dmax* with observed values. *Dmax* are calculated as the maximum slip in the row of the 1x1 km subfaults at zero depth. Observed values are re-examined data for strike-slip events from [31, 32]. Simulation results (red triangles) correlate well with observed data (black dots).

In Fig.10 we compare scaling relations *S*(*Mo*) and *Dave*(*Mo*) with observed ones. In average, agreement is good, but a step-like change is noticeable at the boundary between the 1st and 2nd stages at *Mw*=6.5: *S* and *Dave* values in 2nd stage have good fit, while ruptures in the 1st stage have underestimated *S* and overestimated *Dave* values. Comparison with Fig.9 demonstrate that ruptures in the 2nd stage have surface rupture, while ruptures in the 1st stage are buried, in accordance with the W-model and self-similar model of scaling. From Fig.10 we may infer also that buried ruptures have larger Δσ than surface ruptures [33, 34].

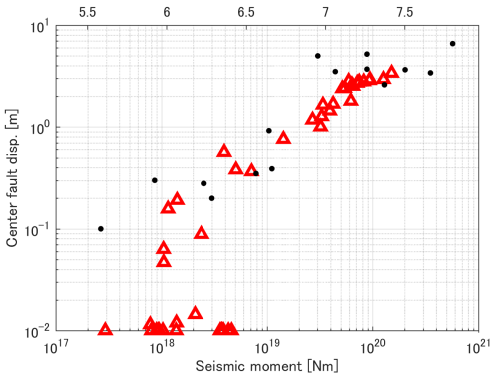

Fig. 9 – Comparison of simulated (triangles) and observed (dots) values of the permanent surface offset for Case 5

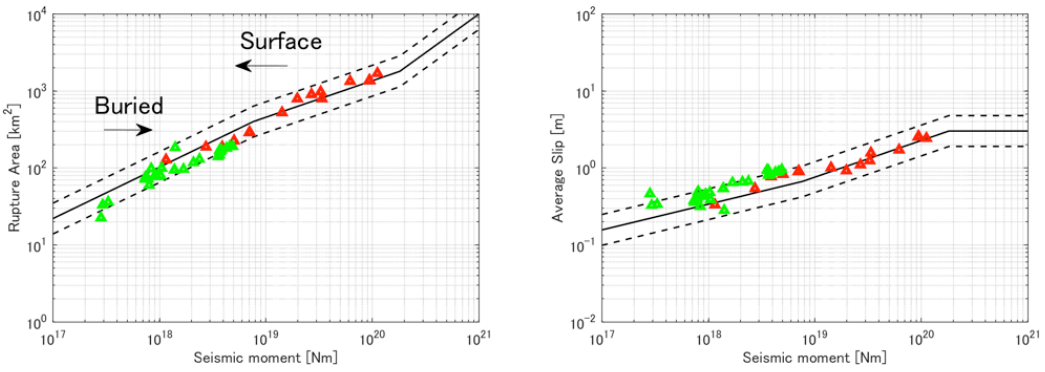

Fig.10 – Scaling of the rupture area *S* (left) and average slip *Dave* (right) for Case 5. In this plot the buried ruptures are marked by green triangles, and surface ruptures by red triangles. Arrows indicate estimates of buried and surface rupture ranges for recent earthquakes in Japan [36].

5. Discussion

In [1] we made similar simulations for ruptures in the transition from the 2nd to 3rd stage. However, friction settings are different. We need to unify parameter settings for both simulations. Driven by results in Table 2 we can try to find common parameter settings that allow us to reproduce both scaling relations and observed ground motions in all 3 stages.

Assuming a uniform distribution of *Dc* having short correlation length made our simulations more irregular than before. However, slip distributions are still smooth in comparison with observed slip distributions. Heterogeneities of other parameters of RS friction may be necessary. For example, considering that fault walls have geometrically rough (not smooth) surfaces, the fault gouge can be thinner in their contacts and thicker in the places where the walls move away from one another. We expect normal stress to be larger in places of contact and smaller in other places, e.g. [35].

Simulated events are a valuable data set for the study of detailed features of rupture models. Our preliminary studies indicate that there may be significant correlations between slip rate, rise time, rupture velocity and *Dc* distribution. There are also indications that the locations of high-slip-rate areas are correlated with locations of high-slip areas, having the following order in space: rupture initiation – high-slip area – high-slip-rate area. These are analyzed in the companion paper [2].

After tuning the friction model so that simulated ruptures could reproduce a wide range of observed features of earthquakes, the fully dynamic multicycle methodology, developed here, is a valuable instrument for studying aspects of earthquake rupture that cannot be directly observed or inferred from source inversion. Except for its large computational cost, this methodology has many advantages in comparison with regular single rupture dynamic simulations, as summarized in [1].

6. Conclusions

A large number of both small and large events with *Mw* 5.5~7.5 were successfully simulated by physics-based full-dynamic multi-cycle earthquake simulations. Scaling relations for rupture area *S* and average slip *Dave* vs. *Mo* clearly confirms a transition between the 1st and 2nd stages. Tuning of normal stress, *Dc_max* and *Wseis* also allowed fitting of average values of *S* and *Dave* to observed values. Average $\Delta\sigma$ agrees with the value proposed in Irikura and Miyake (2011): $\Delta\sigma$ = 3MPa.

7. Future work

From this research we understand the importance of the shallow friction settings for rupture propagation. In our next study we will explore multicycle models with different shallow *Dc* and other friction parameters,

and explore ruptures with depth dependence of slip rate functions and other rupture parameters as well. In this new study we will keep our approach: earthquake cycle simulation – validation – analysis of validated ruptures. Additionally, we will make similar analysis for the 3rd stage and for other types of faults such as reverse faults.

8. Acknowledgements

This study is based on the 2018 research project 'Examination for uncertainty of strong ground motion prediction for inland crustal earthquakes' by the Secretariat of Nuclear Regulation Authority (NRA), Japan. The Super Computer Shaheen II at KAUST University has been used to run the models presented in this study.

9. References

[1] Galvez P, Somerville P, Petukhin A, Ampuero JP, Peter D (2019a): Earthquake Cycle Modelling of Multi-segmented Faults. Dynamic Rupture and Ground Motion Simulation for the 1992 Mw 7.3 Landers Earthquake. *Pure Appl. Geophys.*, doi:10.1007/s00024-019-02228-x.

[2] Petukhin A, Galvez P, Somerville P, Miyakoshi K, Irikura K, (2020): Analysis and Validation of Heterogeneous Dynamic Ruptures Modeled by Earthquake Cycle Simulation. *17th World Conference on Earthquake Engineering, September 13-18, Sendai, Japan*, Paper N°C001918, submitted.

[3] Irikura K, Miyake H (2011): Recipe for predicting strong ground motion from crustal earthquake scenarios. *Pure Appl. Geophys.*, **168**, 85, doi:10.1007/s00024-010-0150-9.

[4] Tullis TE (2012): Preface to the focused issue on earthquake simulators. *Seismological Research Letters*, **83**, 957–958.

[5] Matsu'ura M (2005): Quest for predictability of geodynamic processes through computer simulation. *Computing in Science and Engineering*, **7** (4), 43.

[6] Hillers G, Ben-Zion Y, Mai PM (2006): Seismicity on a fault with rate- and state-dependent friction and spatial variations of the critical slip distance. *J. Geophy. Res.*, **111,** 2156, doi: 10.1029/2005JB003859.

[7] Hillers G, Mai PM, Ben-Zion Y, Ampuero JP, (2007): Statistical properties of seismicity of fault zones at different evolutionary stages. *Geophys. J. Int.*, **169**, 515.

[8] Dieterich JH, Kilgore BD (1994): Direct observation of frictional contacts: New insights for state-dependent properties. *Pure Appl. Geophys.*, **143**, 283, doi:10.1007/BF00874332.

[9] Dieterich JH (1979): Modeling of Rock Friction, 1. Experimental results and constitutive equations. *J. Geophy. Res.*, **84**, 2161.

[10] Ruina, A., "Slip Instability and State Variable Friction Laws", J. Geophys. Res., **88** (1983) 10359.

[11] Galvez P, Ampuero JP, Dalguer LA, Somala SN, Nissen-Meyer T. (2014): Dynamic earthquake rupture modelled with an unstructured 3D spectral element method applied to the 2011 M9 Tohoku earthquake. *Geophys. J. Int.*, **198**, 1222.

[12] Galvez P, Dalguer LA, Ampuero JP, Giardini G (2016): Rupture reactivation during the 2011 Tohoku earthquake: Dynamic rupture and ground motion simulations. *Bull. Seismol. Soc. Am.*, **106,** 819, doi:101785/0120150153.

[13] Luo Y, Ampuero JP, Miyakoshi K, Irikura K (2017): Source rupture effects on earthquake moment-area scaling relations. *Pure Appl. Geophys.*, **174**, 3331, doi: 10.1007/s00024-017-1467-4.

[14] Ida Y (1972): Cohesive force across the tip of a longitudinal shear crack and Griffith's specific surface energy. *J. Geophys. Res.*, **77,** 3796.

[15] Andrews DJ (1976): Rupture propagation with finite stress in antiplane strain. *J. Geophys. Res.*, **81**, 3575.

[16] Pitarka A, (1999): 3D elastic finite-difference modeling of seismic motion using staggered grids with nonuniform spacing. *Bull. Seismol. Soc. Am.*, **89**, 54.

[17] Dalguer LA, Day SM (2007): Staggered-grid split-node method for spontaneous rupture simulation. *J. Geophys. Res.*, **112**, B02302, doi:10.1029/2006JB004467.

[18] Cocco M, Bizzary A (2002): On the slip-weakening behavior of rate- and state dependent constitutive laws. *Geophys. Res. Lett.*, **29**, 1561.

[19] Schmedes J, Archuleta RJ, Lavallee D (2010): Correlation of earthquake source parameters inferred from dynamic rupture simulations. *J.Geophys.Res.*, **115**, B03304, doi:10.1029/2009JB006689.

[20] Field EH (2019): How physics-based earthquake simulators might help improve earthquake forecasts. *Seismol. Res. Lett.*, doi.org/10.1785/0220180299.

[21] Luo Y, Ampuero JP (2015): Multicycle Dynamic simulations of Fault Parameters of Inland Faults, *Progress report, Secretariat of Nuclear Regulation Authority (NRA), Japan*.

[22] Irikura K, Miyake H (2001): Prediction of strong ground motions for scenario earthquakes. *Journal of Geography (Chigaku Zasshi)*, 110(6), 849–875.

[23] Song, S.G., Dalguer, L.A., "Importance of 1-point statistics in earthquake source modeling for ground motion simulation", Geophys. J. Int. 192 (2013) 1255, doi: 10.1093/gji/ggs089.

[24] Galvez P, Petukhin A, Irikura K, Somerville P (2019b): Dynamic Source Model for the 2011 Tohoku Earthquake in a Wide Period Range Combining Slip Reactivation with the Short-Period Ground Motion Generation Process. *Pure Appl. Geophys.*, doi.org/10.1007/s00024-019-02210-7

[25] Sibson RH (1992): Implications of fault-valve for the rupture nucleation and recurrence. *Tectonophysics*, **211**, 283–293.

[26] Streit JE, Cox SF (2001): Fluid pressures at hypocenters of moderate to large earthquakes. *Journal of Geophysical Research*, **106**, 2235–2243.

[27] Mai PM, Beroza GC (2002): A spatial random field for the characterize complexity in earthquake slip. *J. Geophys. Res.*, **107**, doi:10.1029/2001JB000588.

[28] Somerville P, Irikura K, Graves R, Sawada S, Wald D, Abrahamson N, et al. (1999): Characterizing crustal earthquake slip models for the prediction of strong ground motion. *Seism. Res. Lett.*, **70**, 59-80.

[29] Fujii Y, Matsu'ura M (2000): Regional Difference in Scaling Laws for Large Earthquakes and its Tectonic Implication. *Pure Appl. Geophys.*, **157**, 2283–2302.

[30] Ampuero JP, Rubin AM (2008): Earthquake nucleation on rate and state faults – Aging and slip laws. *J. Geophys. Res.*, **113**, B01302.

[31] Stirling M, Rhoades D, Berryman K (2002): Comparison of earthquake scaling relations derived from data of the instrumental and pre-instrumental era. *Bull. Seismol. Soc. Am.*, **92**, 812–830.

[32] Murotani S, Matsushima S, Azuma T, Irikura K, Kitagawa S (2015): Scaling Relations of Source Parameters of Earthquakes Occurring on Inland Crustal Mega-Fault Systems. *Pure Appl. Geophys.*, **172**, 1371–1381.

[33] Somerville PG (2003): Magnitude scaling of the near fault rupture directivity pulse, *Phys. Earth Planet. Int.*, **137**, 201–212.

[34] Kagawa T, Irikura K, Somerville PG (2004): Differences in ground motion and fault rupture process between the surface and buried rupture earthquakes. *Earth Planets Space*, **56**, 3–14.

[35] Ozawa SW, Hatano T, Kame N (2019): Longer Migration and Spontaneous Decay of Aseismic Slip Pulse Caused by Fault Roughness. *Geophys. Res. Lett.*, doi: 10.1029/2018GL081465.

[36] Azuma T, Maruyama T (2016): Investigation of surface deformation associated with the 2016 Tottori-ken Chubu Earthquake (Mj6.6). *IEVG newsletter*, **3**(5), National Institute of Advanced Industrial Science and Technology, Japan.

